*J. Fluid Mech.* (2007), *vol.* 574, *pp.* 155–167.  
doi:10.1017/S0022112006003788 Printed in the United Kingdom

# Spatial signatures of retrograde spanwise vortices in wall turbulence

V. K. NATRAJAN, Y. WU AND K. T. CHRISTENSEN†

Department of Mechanical Science and Engineering, University of Illinois, Urbana, IL 61801, USA

(Received 20 April 2006 and in revised form 10 October 2006)

The spatial signatures of retrograde spanwise vortices in wall turbulence are assessed from particle-image velocimetry measurements in the streamwise–wall-normal plane of a zero-pressure-gradient turbulent boundary layer at $Re_\tau \equiv u_*\delta/\nu = 2350$. The present results suggest that a proportion of retrograde spanwise vortices have a well-defined spatial relationship with neighbouring prograde vortices. Two-point cross-correlations and conditionally averaged velocity fields given a retrograde vortex reveal that such structures are typically oriented either upstream of and below or downstream of and above a prograde core. While these pairings are consistent with the typical-eddy patterns reported by Falco and co-workers, we offer an alternative interpretation for a proportion of these retrograde/prograde pairs. In particular, the arrangement of a retrograde spanwise vortex upstream of and below a prograde core is also consistent with the spatial signature revealed if an omega-shaped hairpin structure were sliced through its shoulder region by a fixed streamwise–wall-normal measurement plane.

## 1. Introduction

Many studies support the existence of hairpin-like structures in wall-bounded turbulent flows (Theodorsen 1952; Head & Bandyopadhyay 1981; Smith *et al.* 1991; Zhou *et al.* 1999; Adrian, Meinhart & Tomkins 2000; Ganapathisubramani, Longmire & Marusic 2003, among many others). The last four efforts also reveal that these vortices streamwise-align to form larger-scale structures termed vortex packets that are characterized by an inclined interface formed by the heads of the structures as well as a region of large-scale streamwise momentum deficit beneath the interface due to the collective induction of the vortices. When sliced in the streamwise–wall-normal plane, the heads of the individual hairpins appear as spanwise vortex cores with $\omega_z < 0$, where $\omega_z$ is the fluctuating spanwise vorticity, and strong ejections of low-speed fluid are observed upstream of and below each head due to the collective induction of the hairpin's head and leg(s). Spanwise vortices for which $\omega_z < 0$ are termed prograde spanwise vortices herein since their rotation is in the same sense as the mean shear. Recent work by Wu & Christensen (2006) shows that the largest populations of prograde spanwise vortices, most of which bear spatial signatures consistent with hairpin heads, occur in the region $y < 0.3\delta$.

Retrograde spanwise vortices, positive $\omega_z$ cores, have also been observed in wall turbulence. Falco (1977, 1983, 1991) present evidence of 'typical eddies' in the outer region which have spatial characteristics consistent with ring-like structures. The flow

† Author to whom correspondence should be addressed: ktc@uiuc.edu.

visualizations and an idealized schematic of these structures in Falco (1977) show that typical eddies appear as spatially coincident prograde and retrograde spanwise vortices when sliced in the streamwise–wall-normal plane. Falco (1977, 1983, 1991) offer little discussion regarding a preferred orientation for typical eddies except to state that the idealized schematic in Falco (1977) (which portrays the prograde core above and slightly downstream of the retrograde core) represents the "commonly-observed view" of such a structure in the streamwise–wall-normal plane. More recently, Klewicki & Hirschi (2004) observed that near-wall shear layers often occur in close proximity to clusters of prograde structures as well as adjacent regions of opposing-sign $\omega_z$, with the retrograde event either above or below the prograde event.

The generation of such ring-like structures may be related to the pinch-off and reconnection of the legs of existing hairpin structures as observed by Moin, Leonard & Kim (1986), Smith *et al.* (1991) and Bake, Meyer & Rist (2002). Alternatively, Tomkins & Adrian (2003) proposed the generation of isolated retrograde structures via the spanwise merger of hairpin structures. Another possibility is that some fraction of retrograde structures occur in tandem with an adjacent prograde structure via a single streamwise-aligned vortex structure, possibly a hairpin. Hambleton, Hutchins & Marusic (2006) computed a linear stochastic estimate of the conditionally averaged fluctuating velocity field given a retrograde spanwise vortex at $y = 0.4\delta$ in the streamwise–wall-normal plane and observed a prograde spanwise vortex positioned downstream of (by $0.5\delta$) and above (at $y \approx \delta$) the retrograde core. They conjectured this pattern to be the imprint of a slice through a large-scale vortex ring or omega-shaped vortex loop. Hambleton *et al.* (2006) also noted that estimates of similar fields for retrograde vortices closer to the wall did not yield spatially coincident prograde cores. Regardless of their origin, Wu & Christensen (2006) report that retrograde spanwise vortices occur most frequently in the region $0.15\delta < y < 0.25\delta$, although prograde spanwise vortices are still found to outnumber retrograde cores by approximately 2:1 in this wall-normal region. In addition, few retrograde structures were identified at the inner boundary of the log layer. Finally, that work reveals an increase in the fraction of retrograde structures relative to prograde vortices in the outer layer with Reynolds number ($Re$), indicating that such structures may play an increasingly important role at higher $Re$. The present effort documents the spatial signatures of retrograde spanwise vortices and explores their relationship with neighbouring prograde cores.

## 2. Experiment

The experimental data utilized herein is a subset of measurements reported by Wu & Christensen (2006). Two-thousand five-hundred instantaneous velocity $(u, v)$ fields were acquired by particle-image velocimetry (PIV) over a $\delta \times \delta$ field of view in the streamwise–wall-normal $(x,y)$ plane of a zero-pressure-gradient turbulent boundary layer at $Re_\tau \equiv u_*\delta/\nu = 2350$. The wind-tunnel facility utilized for these measurements has a documented turbulence intensity of 0.16% in the free stream and the boundary layer develops over a 6.1 m long hydraulically smooth flat plate (Meinhart 1994). The friction velocity, $u_* = \sqrt{\tau_w/\rho}$, and the viscous length scale, $y_* = \nu/u_*$, were determined using the Clauser chart method. The PIV images were interrogated using two-frame cross-correlation methods which yielded nearly 35 000 vectors per instantaneous velocity field with vector grid spacings in inner units of $\Delta x^+ = \Delta y^+ = 12.3$. Table 1 summarizes the relevant flow parameters and the reader is directed to Wu & Christensen (2006) for further experimental details.

| $Re_\tau$ | $Re_\theta$ | $U_\infty$ | $\delta$ | $\theta$ | $u_*$ | $y_*$ | $\Delta x^+$ | $\Delta y^+$ |
|---|---|---|---|---|---|---|---|---|
| — | — | ($\mathrm{m\,s^{-1}}$) | (mm) | (mm) | ($\mathrm{m\,s^{-1}}$) | ($\mu$m) | — | — |
| 2350 | 8330 | 10.0 | 103.1 | 10.1 | 0.36 | 43.9 | 12.3 | 12.3 |

TABLE 1. Summary of boundary layer characteristics and experimental parameters.

## 3. Instantaneous evidence

Determining the spatial characteristics of retrograde spanwise vortices requires effective visualization of such structures in the instantaneous velocity realizations. While Galilean decomposition reveals vortices advecting at a fixed advection velocity ($U_c$) and is often most effective when one wishes to visualize the local motions induced by vortices, it is of less use as a global identification tool when the advection velocities of the structures have spatial dependence. Alternatively, embedded structure can be revealed in a Galilean-invariant manner through analysis of the local velocity gradient tensor. One such technique is swirling strength ($\lambda_{ci}$) – the imaginary part of the complex eigenvalue of the local velocity gradient tensor (Zhou *et al.* 1999). While $\lambda_{ci}$ does not retain the rotational sense of the identified swirling motion, one can define

$$\Lambda_{ci}(x, y) = \lambda_{ci}(x, y)\frac{\omega_z(x, y)}{|\omega_z(x, y)|}, \tag{3.1}$$

which assigns the sign of the fluctuating spanwise vorticity to $\lambda_{ci}$, facilitating differentiation between prograde ($\Lambda_{ci} < 0$) and retrograde ($\Lambda_{ci} > 0$) spanwise vortices.

Identifying the boundaries of individual vortices using $\Lambda_{ci}$ requires a suitable threshold. Wu & Christensen (2006) found that a universal threshold, independent of both $y$ and $Re$, can be achieved through normalization of $\Lambda_{ci}(x, y)$ with its root-mean-square (RMS), $\Lambda_{ci}^{\mathrm{rms}}(y)$ (a similar threshold definition is offered by Nagaosa & Handler (2003) for vortex identification via the second invariant of $\nabla\mathbf{u}$). A threshold of $|\Lambda_{ci}(x, y)|/\Lambda_{ci}^{\mathrm{rms}}(y) \geqslant 1.5$ was found to effectively define the boundaries of vortex cores while minimizing the influence of experimental noise associated with calculation of the velocity gradients (the reader is directed to Wu & Christensen (2006) for a more complete discussion of this methodology). Both Galilean decomposition and $\Lambda_{ci}$ with this threshold are employed herein to study the spatial signatures of retrograde spanwise vortices.

Figure 1(*a*) presents a representative Galilean-decomposed instantaneous velocity field in the streamwise–wall-normal plane of a turbulent boundary layer at $Re_\tau = 2350$, with the associated $\Lambda_{ci}$ field presented as figure 1(*b*). Several prograde and retrograde spanwise vortices are visible in the Galilean decomposition, each of which has a cluster of non-zero $\Lambda_{ci}$ associated with it. Five streamwise-aligned prograde vortices (labelled A–E) are noted near $(x, y) = (0.25\delta, 0.1\delta)$ with each vortex exhibiting a strong ejection of fluid away from the wall just below and upstream of its core. These spatial characteristics are consistent with the hairpin vortex signature suggested by Adrian *et al.* (2000), indicating that these prograde spanwise vortices are the heads of hairpin vortices. This train of vortices forms a tent-like interface and a large-scale region of streamwise momentum deficit is observed below the interface due to the collective induction of the vortices, consistent with the vortex-packet observations of Adrian *et al.* (2000). In addition, several other $\Lambda_{ci}$ clusters are noted in figure 1(*b*) at locations where swirling motions are not observed in the velocity field. These clusters

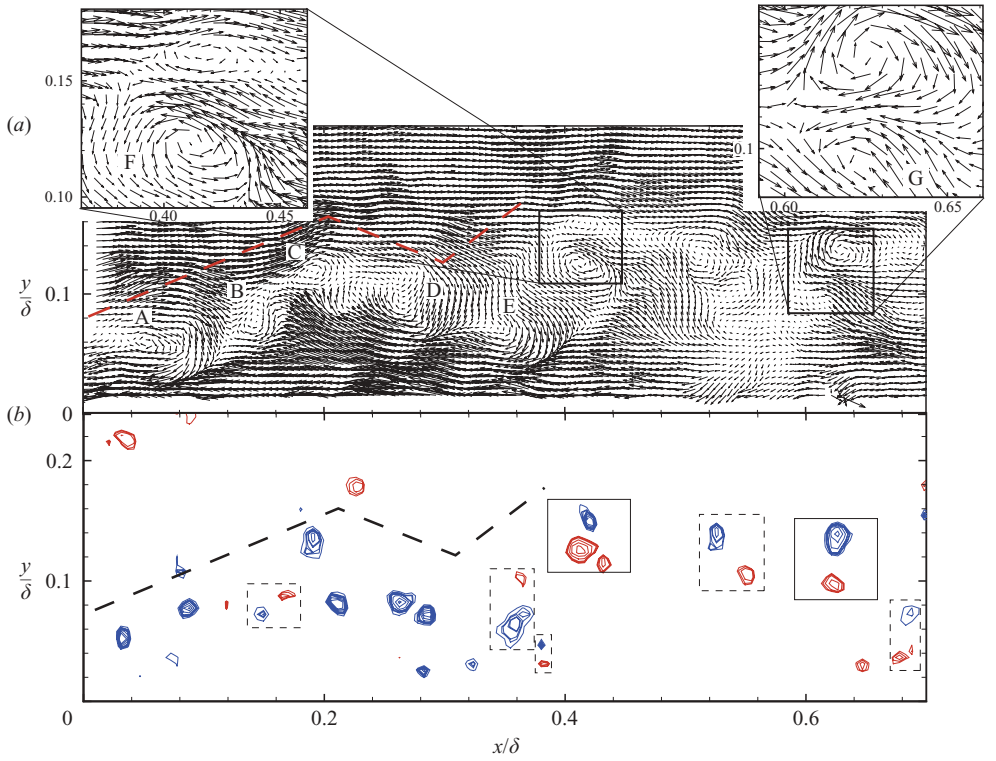


FIGURE 1. (*a*) Galilean-decomposed velocity field in the streamwise–wall-normal plane at $Re_\tau = 2350$ with $U_c = 0.81U_\infty$. (*b*) Retrograde (red) and prograde (blue) $\Lambda_{ci}$ calculated from the velocity field in (*a*). The dashed line highlights the tent-like interface of the visualized packet.

represent spanwise vortices that are not moving with the advection velocity chosen for the Galilean decomposition.

Two retrograde vortices are also revealed in figure 1 (labelled F and G). The insets of figure 1(*a*) present enlarged views of the local velocity fields around these two retrograde vortices, with each retrograde structure appearing in close proximity to a prograde vortex just above and downstream of its core. Further, while a few isolated retrograde structures are apparent in the $\Lambda_{ci}$ field, a majority of them appear in close proximity to prograde cores in various orientations. Several possible pairings are highlighted in figure 1(*b*) using dashed-line bounding boxes, with the orientation of a retrograde core upstream of and below a prograde core occurring most often in this realization. In contrast, many of the prograde vortices occur in isolation rather than in tandem with retrograde structures.

## 4. Statistical evidence

### 4.1. *Two-point correlations*

Two-point spatial correlations between the swirling strengths of prograde and retrograde vortices are calculated to further explore the spatial characteristics of retrograde cores, particularly their relationship with neighbouring prograde vortices.

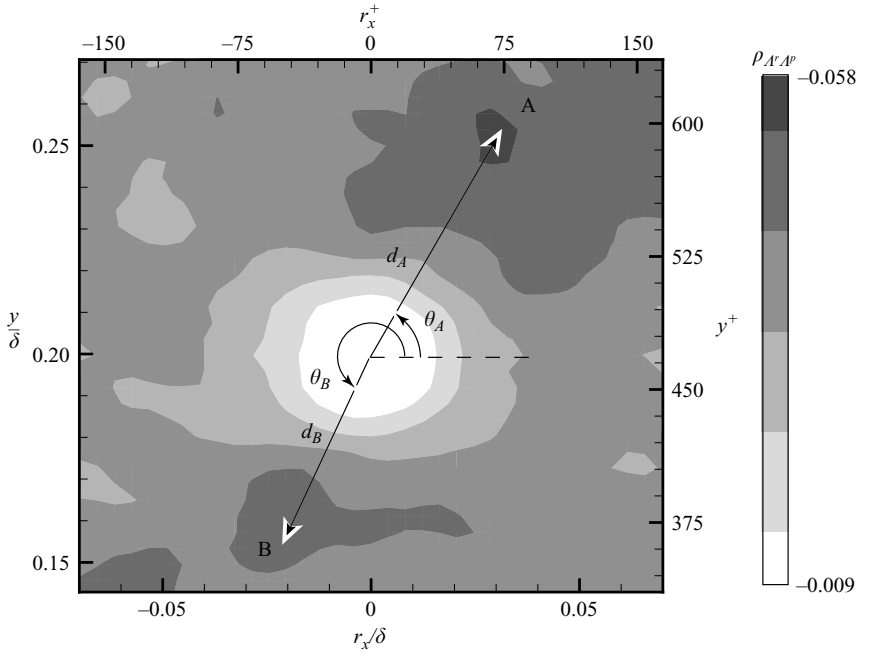


FIGURE 2. Two-point cross-correlation coefficient between $\Lambda_{ci}^r$ and $\Lambda_{ci}^p$, $\rho_{\Lambda^r\Lambda^p}$, at $y_{\mathrm{ref}} = 0.2\delta$.

Each instantaneous $\Lambda_{ci}$ field is divided into a prograde field as

$$\Lambda_{ci}^p(x, y) = \begin{cases} \Lambda_{ci}(x, y) & \text{if } \Lambda_{ci}(x, y) \leqslant -1.5\Lambda_{ci}^{\mathrm{rms}}(y), \\ 0 & \text{otherwise,} \end{cases} \tag{4.1}$$

and a retrograde field as

$$\Lambda_{ci}^r(x, y) = \begin{cases} \Lambda_{ci}(x, y) & \text{if } \Lambda_{ci}(x, y) \geqslant +1.5\Lambda_{ci}^{\mathrm{rms}}(y), \\ 0 & \text{otherwise,} \end{cases} \tag{4.2}$$

using the aforementioned threshold, which yields efficient separation of prograde and retrograde cores and facilitates calculation of the two-point cross-correlation coefficient

$$\rho_{\Lambda^r\Lambda^p}(r_x, y) = \frac{\left\langle \Lambda_{ci}^r(x, y_{\mathrm{ref}})\Lambda_{ci}^p(x + r_x, y)\right\rangle}{\sigma_{\Lambda^r}(y_{\mathrm{ref}})\sigma_{\Lambda^p}(y)}, \tag{4.3}$$

where $\sigma_{\Lambda^r}$ and $\sigma_{\Lambda^p}$ are the RMS of $\Lambda_{ci}^r$ and $\Lambda_{ci}^p$, respectively.

Given that the largest populations of retrograde vortices occur in the range $0.15\delta < y < 0.25\delta$ (Wu & Christensen 2006), figure 2 presents $\rho_{\Lambda^r\Lambda^p}$ at $y_{\mathrm{ref}} = 0.2\delta$. The cross-correlation coefficient is zero at the event location and negative elsewhere, as expected, since we are cross-correlating retrograde swirl with prograde swirl. The cross-correlation coefficient also displays two definitive, yet broad, regions of enhanced correlation which represent preferred orientations of prograde structures relative to retrograde cores. The first region occurs in quadrant one of this plot, downstream of and above the event location $(r_x, y) = (0, y_{\mathrm{ref}})$, and its position of maximum correlation is denoted 'A' in figure 2. The second region of enhanced correlation (labelled 'B') is weaker than the first and occurs in quadrant three – upstream of and below the event location. One can approximate these orientations by a 'mean'

radial distance from the event location, $d$, and a 'mean' angle relative to horizontal, $\theta$, yielding $d_A^+ = 135$ ($d_A = 0.058\delta$) and $\theta_A = 65°$ for peak location A and $d_B^+ = 103.5$ ($d_B = 0.044\delta$) and $\theta_B = 230°$ for peak location B. However, it should be noted that both regions of correlation span regions that are broad in both angle ($30° < \theta_A < 90°$ and $210° < \theta_B < 290°$) and distance relative to the reference location, indicating that the relative angle and spacing between correlated instantaneous retrograde and prograde structures can fluctuate.

While the magnitude of $\rho_{\Lambda^r\Lambda^p}$ is small at A and B in figure 2 compared to the limiting case of perfect correlation between spatially correlated instantaneous prograde and retrograde structures in these orientations ($\rho_{\Lambda^r\Lambda^p} \approx -0.5$), this limiting case would only be possible if the angle and spacing between the structures were identical for all instantaneous pairs and there were no uncorrelated prograde and/or retrograde structures in the vicinity to generate de-correlation. Clearly such an ideal case should not be expected in a flow that is marked by strong turbulent fluctuations. As such, fluctuations in the angle and spacing between spatially correlated instantaneous prograde and retrograde structures should be expected and probably account for the relatively low values of $\rho_{\Lambda^r\Lambda^p}$ observed in figure 2. This hypothesis is validated by considering a model problem in which a large ensemble of artificial $\Lambda_{ci}^r$ and $\Lambda_{ci}^p$ fields is generated wherein only spatially correlated retrograde and prograde spanwise vortices are present and oriented at angles and distances equal to the positions of peaks A and B in figure 2 (50% at each orientation for simplicity). Slight random fluctuations of $\pm 7.5°$ about $\theta_A$ and $\theta_B$ and $\pm 0.015\delta$ about $d_A$ and $d_B$ are then imposed for each vortex pair and the two-point correlation coefficient is computed. While idealized, this model problem yields values and spatial extents of $\rho_{\Lambda^r\Lambda^p}$ consistent with those presented in figure 2 ($\rho_{\Lambda^r\Lambda^p} = -0.098$ for the model problem compared to $\rho_{\Lambda^r\Lambda^p} = -0.06$ for peak A in figure 2, for example). This consistency substantiates the interpretation of peaks A and B as mean preferred orientations of prograde spanwise vortices relative to retrograde cores about which slight fluctuations in angle and spacing are observed.

### 4.2. *Spatial orientations of neighbouring retrograde and prograde vortices*

Given the preferred spatial orientations of prograde vortices relative to retrograde cores observed in $\rho_{\Lambda^r\Lambda^p}$, this relationship is explored further by considering histograms of the spacing ($d$) and angular orientation ($\theta$) of instantaneous, spatially coincident retrograde and prograde vortices. Each retrograde vortex at $y = 0.2\delta$ in the instantaneous $\Lambda_{ci}$ fields is identified, its closest prograde neighbour is determined, and the spacing and angular orientation of the prograde core relative to the retrograde vortex are then assessed. Figures 3($a$) and 3($b$) present histograms of $d$ and $\theta$, respectively, at $y = 0.2\delta$. Distances in the range $50 < d^+ < 200$ ($0.021 < d/\delta < 0.085$) are observed with a peak near $d^+ = 100$ ($d = 0.042\delta$), while broad peaks in the angle histogram occur at approximately $\theta = 70°$ and 260°. These characteristics are consistent with the character of $\rho_{\Lambda^r\Lambda^p}$.

### 4.3. *Conditionally averaged velocity fields*

Conditionally averaged velocity fields given the presence of a retrograde vortex are also computed to uncover its average velocity signature. These averages are accomplished by centring a bounding box of width and height $0.2\delta$ around each identified retrograde vortex at $y = 0.2\delta$ and the local velocity field contained within this box is extracted. The instantaneous advection velocity of each identified retrograde vortex is removed, yielding the local velocity field in the reference frame of the retrograde core. Since figures 2 and 3($b$) reveal clear orientation preferences between retrograde and prograde structures, the identified retrograde vortices are sorted into four ensembles

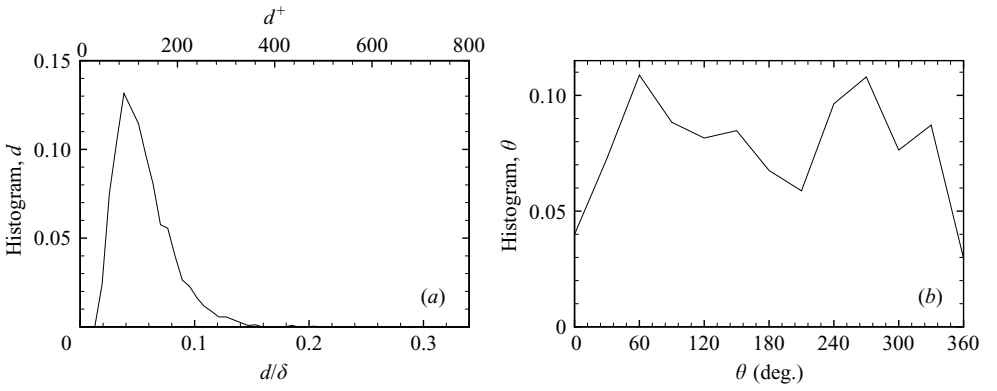


FIGURE 3. Histograms of (*a*) spacing, $d$, and (*b*) angular orientation, $\theta$, between identified retrograde spanwise vortices at $y = 0.2\delta$ and their closest prograde neighbours.

based upon the angular orientation of their closest prograde neighbour: $0^\circ \leqslant \theta < 90^\circ$, $90^\circ \leqslant \theta < 180^\circ$, $180^\circ \leqslant \theta < 270^\circ$ and $270^\circ \leqslant \theta < 360^\circ$ (hereafter referred to as quadrants one to four, respectively). Conditional averages are then computed for each orientation subset.

Figure 4(*a–d*) presents conditionally averaged velocity fields for retrograde vortices centred at $y = 0.2\delta$ computed for each of the quadrants given above. We first consider the conditionally averaged velocity field for a retrograde spanwise vortex whose closest prograde neighbour resides in quadrant one. This subset constitutes approximately 26% of the total number of identified retrograde vortices at $y = 0.2\delta$ (1401 retrograde vortices in total) and the corresponding conditionally averaged velocity field presented in figure 4(*a*) reveals a well-defined prograde vortex oriented downstream of and above the retrograde core at an angle of approximately 47° and spacing of $103y_*$ ($= 0.044\delta$). This orientation is consistent with the preferences noted in $\rho_{\Lambda^r \Lambda^p}$ and the histograms of spacing and angular orientation. In addition, this spatial velocity signature is quite similar to that observed for the retrograde structures identified in figure 1(*a*). As such, a clear preference exists for some retrograde vortices at $y = 0.2\delta$ to be oriented below and upstream of neighbouring prograde cores.

The conditionally averaged velocity field for the quadrant-three orientation, for which both $\rho_{\Lambda^r \Lambda^p}$ and the histograms of spacing and orientation reveal a preference, is presented in figure 4(*c*). The retrograde samples included in this average comprise roughly 26% of the retrograde vortices at $y = 0.2\delta$ and the conditional average reveals a well-defined prograde vortex below and upstream of the retrograde core with a relative spacing of $0.046\delta$ ($=108y_*$) at an angle of 220°. Finally, the quadrant-two (figure 4*b*) and quadrant-four (figure 4*d*) ensembles, which account for 25% and 23% of the retrograde vortices at $y = 0.2\delta$, respectively, reveal average velocity fields devoid of prograde vortices.

While the velocity fields in figure 4 indicate that retrograde vortices are often related to neighbouring prograde vortices oriented in quadrants one and three with a spacing of approximately $100y_*$, it is not clear whether the opposite is true. That is, do a majority of prograde vortices occur in tandem with neighbouring retrograde structures? While most of the instantaneous prograde spanwise vortices observed in figure 1 appear to occur in isolation, conditional averages are computed to further explore this possibility. Figures 5(*a*) and 5(*b*) present conditionally averaged velocity fields given a prograde vortex at $y = 0.2\delta$ oriented in quadrants one and three,

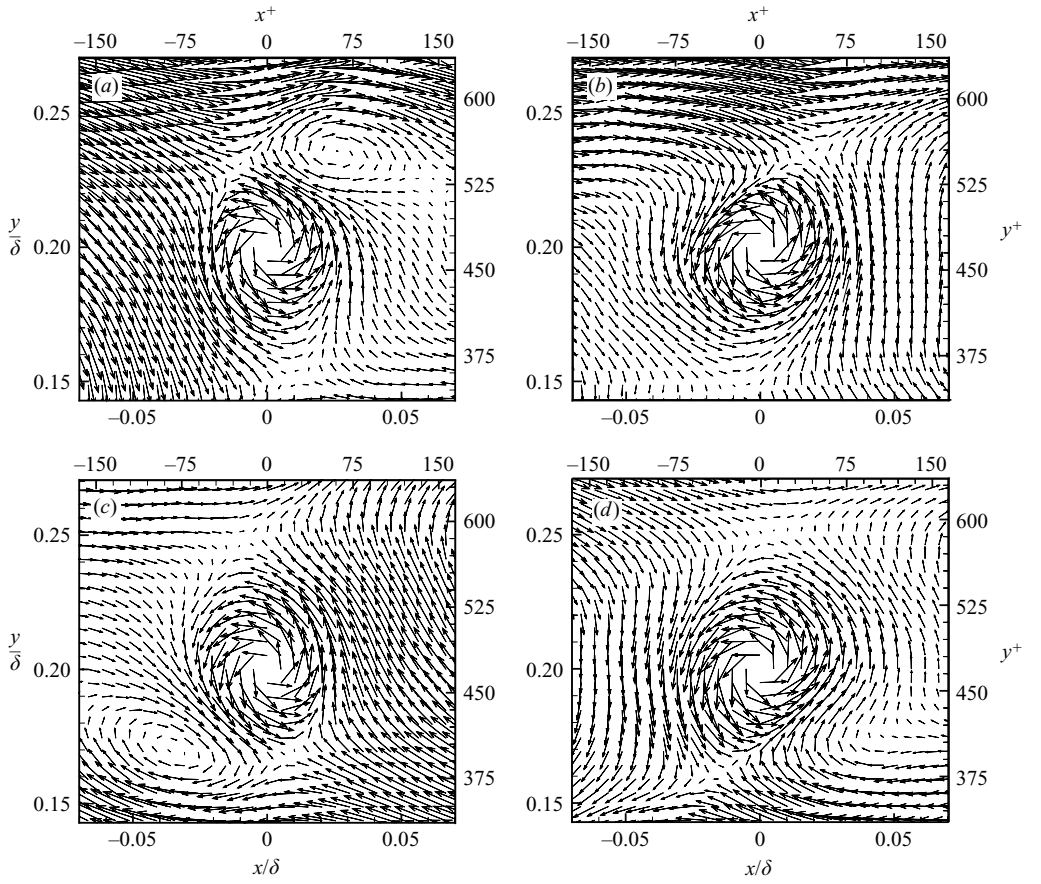


FIGURE 4. Conditionally averaged velocity fields given a retrograde vortex at $y = 0.2\delta$ for which its closest prograde vortex is oriented in quadrants (*a*) one, (*b*) two, (*c*) three and (*d*) four relative to the retrograde core.

respectively, relative to their closest retrograde neighbours. (Given the patterns noted in figure 4, only quadrant one and three orientations are presented. The quadrant two and four subsets yield similar patterns.) Each of these conditionally averaged prograde structures displays a closed streamline pattern with clockwise rotation and a strong ejection of low-speed fluid away from the wall, consistent with the hairpin vortex signature offered by Adrian *et al.* (2000); however, each field is devoid of retrograde structures.

However, when these prograde conditional averages are further restricted to only include those prograde vortices that are within $150y_*$ of their closest retrograde neighbour, based on the results in figures 2–4, a different pattern emerges. Figure 5(*c*) presents this conditional average for the quadrant-one orientation and reveals a retrograde vortex oriented at approximately 240° relative to the prograde vortex core (or equivalently a prograde structure oriented at approximately 60° relative to the retrograde core). This velocity signature is nearly identical to that observed in the conditionally averaged velocity field given a retrograde vortex with its closest prograde neighbour in quadrant one (figure 4*a*). In contrast, the conditionally averaged field for a prograde vortex oriented in quadrant three relative to its closest retrograde

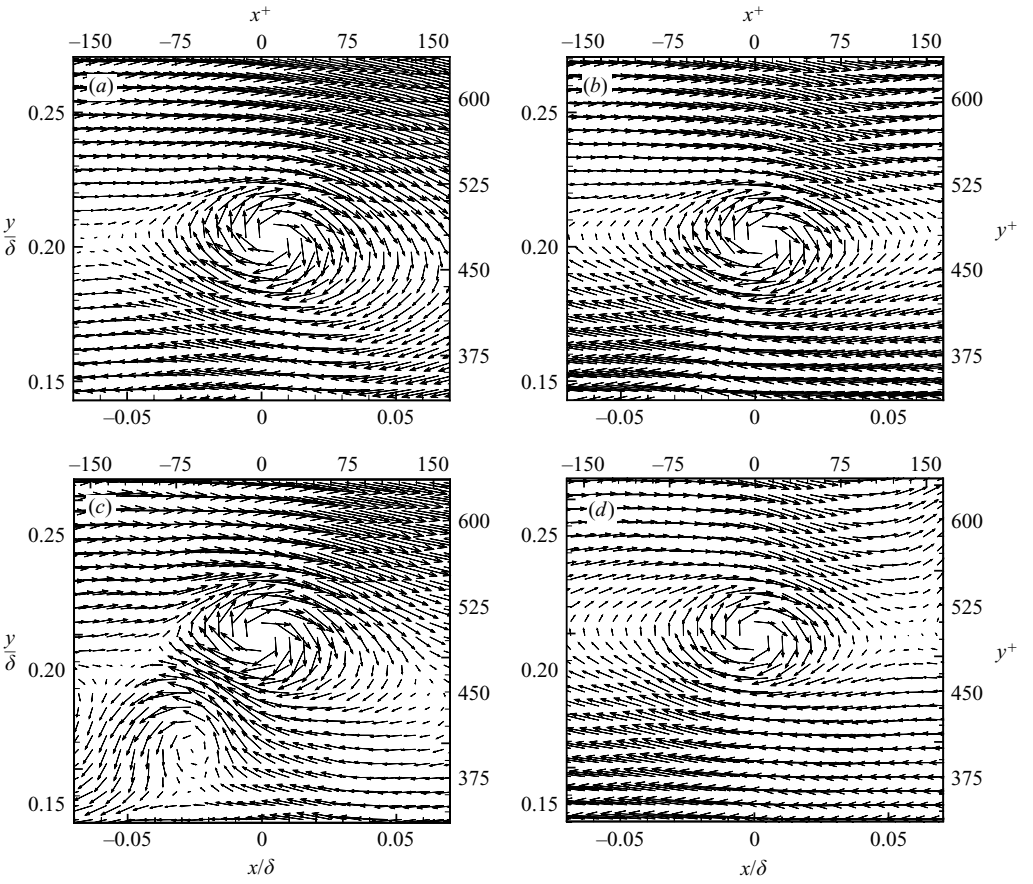


FIGURE 5. (*a*,*b*) Conditionally averaged velocity fields given a prograde vortex at $y = 0.2\delta$ oriented in quadrants one and three, respectively, relative to its closest retrograde neighbour. (*c*,*d*) Same as (*a*,*b*) except averages are also restricted to prograde/retrograde neighbours spaced within $150y_*$.

neighbour (figure 5*d*) is devoid of a retrograde core and simply resembles the hairpin-vortex signature of Adrian *et al.* (2000). As such, while most prograde vortices in the quadrant-one orientation and within $150y_*$ of their closest retrograde neighbours show a clear orientation preference, most prograde vortices in the quadrant-three orientation are randomly oriented relative to their closest retrograde neighbours.

## 5. Discussion and conclusions

Instantaneous evidence is presented supporting a spatial relationship between retrograde and prograde spanwise vortices near the outer edge of the log layer where the retrograde populations are largest (Wu & Christensen 2006). The present results suggest that many retrograde vortices occur in tandem with neighbouring prograde cores with angular orientations $40^\circ < \theta < 90^\circ$ and $220^\circ < \theta < 290^\circ$ (relative to the retrograde cores) and a mean spacing of approximately $(100\text{–}150)y_*$. These characteristics are observed in spatial cross-correlations of retrograde and prograde swirling strength, histograms of the spacing and angular orientation between identified retrograde vortex cores and their closest prograde neighbour and conditional averages

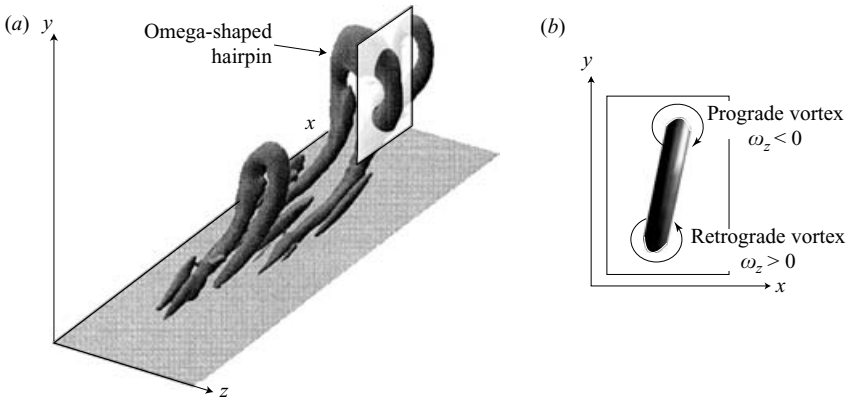


FIGURE 6. (*a*) Three-dimensional visualization of a hairpin vortex packet, adapted from Zhou *et al.* (1999), illustrating the existence of omega-shaped hairpin structures. (*b*) Spatial signature revealed if the structure in (*a*) were sliced through one of its shoulders by a streamwise–wall-normal measurement plane.

of the local velocity fields around identified retrograde vortices. Further, the preferred alignment of retrograde vortices either above or below prograde cores is consistent with the orientations of adjacent regions of opposing-sign $\omega_z$ observed in the vicinity of near-wall shear layers by Klewicki & Hirschi (2004). In contrast, most prograde spanwise vortices occur in isolation, except for a small subset of prograde cores that appear related to retrograde structures oriented upstream of and below and spaced at approximately (100–150)$y_*$ from these prograde cores.

The spatial relationships between retrograde and prograde spanwise vortices reported herein are not inconsistent with the flow-visualization observations of spatially coincident prograde and retrograde cores by Falco and co-workers. As noted earlier, Falco (1977, 1983, 1991) present many flow visualizations and schematics of spatially coincident prograde and retrograde vortex cores in the streamwise–wall-normal plane, nearly always with the prograde core oriented above and downstream of the retrograde core. This arrangement is consistent with one of the preferred orientations presented herein. However, an alternative argument for this orientation preference can be made by supposing that some fraction of these spatially coincident prograde and retrograde cores are related to one another through a single streamwise-aligned, omega-shaped hairpin structure. Evidence supporting the existence of omega-shaped hairpin structures has been presented previously in the literature (Zhou *et al.* 1999; Bake *et al.* 2002, for example).

Figure 6(*a*) presents a three-dimensional visualization of a vortex packet originally reported in Zhou *et al.* (1999, figure 3*c*) that illustrates the possible development of hairpin structures with distinct omega shapes around their shoulders and heads. Similar omega-shaped structures are also presented in Bake *et al.* (2002). If the hairpin in figure 6(*a*) were sliced in the streamwise–wall-normal plane through its spanwise centre, a single prograde spanwise vortex associated with the head of the hairpin would be observed. If, however, this structure were sliced through either of its shoulders, two spanwise vortices would be revealed as illustrated in figure 6(*b*): one with clockwise rotation (a prograde structure) above and downstream of a second vortex core with counterclockwise rotation (a retrograde vortex). While this spatial signature is consistent with the patterns presented in the insets of figure 1(*a*) and the conditionally averaged velocity field of figure 4(*a*), the probability that this orientation

is indeed associated with the shoulder of an omega-shaped hairpin is strengthened by the velocity pattern observed in the conditionally averaged field given a prograde vortex oriented in quadrant one relative to its closest retrograde neighbour with a spacing of $150y_*$ or less (figure 5*c*). Indeed, the prospect of slicing through the shoulder of an omega-shaped hairpin on occasion in a fixed streamwise–wall-normal flow visualization or PIV measurement is certainly a reasonable one given that a preferred spanwise alignment of such structures relative to a fixed measurement plane cannot be expected. In addition, this alternative explanation is not inconsistent with the observations of Falco and co-workers since significant evidence exists that hairpins can, under certain conditions, pinch off at their legs and reconnect to form ring-like structures (Moin *et al.* 1986; Smith *et al.* 1991; Bake *et al.* 2002). Finally, the recent paper by Hambleton *et al.* (2006) includes a similar interpretation of coincident retrograde and prograde spanwise vortices observed in the estimate of the conditionally averaged velocity field given a retrograde core at $y = 0.4\delta$ as a slice through either a large-scale vortex ring or an omega-shaped vortex loop, but for structures well outside the log layer and of size $O(\delta)$.

With regard to the observations of retrograde vortices above and downstream of prograde cores – the second preferred, albeit weaker, orientation observed herein (figure 4*c*) – there are several potential explanations. The first, and simplest, is that this pattern is the imprint of detached ring-like structures that preferentially align themselves into this particular orientation (possibly due to interactions with the surrounding turbulence and/or the wall). On the other hand, it is also possible that retrograde/prograde pairs in the quadrant-three orientation are not related via a single vortex but rather represent the imprint of two different, yet spatially correlated, vortical structures. In the context of the hairpin-packet paradigm, this pattern could represent the imprint of a hairpin vortex streamwise-aligned behind (upstream of) and slightly below an omega-shaped hairpin structure in a coherent vortex packet. In this scenario, the prograde vortex in quadrant three (figure 4*c*) would represent the head of the upstream hairpin while the retrograde vortex would appear as part of the signature of the downstream omega-shaped structure. However, given the packet inclination angle observations of 12°–20° by Adrian *et al.* (2000), estimates of streamwise spacings of vortices in packets of approximately $(0.15–0.2)\delta$ by Christensen *et al.* (2004) at a similar $Re$, and the observed spacing and angle of prograde/retrograde pairs in the quadrant-one orientation, this scenario would yield a quadrant-three orientation with a much larger spacing ($(250–300)y_*$) and a shallower angle (180°–200°) between the vortices compared to that reported herein.

Alternatively, the pinch-off and reconnection of omega-shaped hairpin structures into ring-like vortices also provides a consistent explanation for the quadrant-three orientation. Bake *et al.* (2002) report that as omega-shaped hairpin structures in a transitional boundary layer advect downstream, the head and shoulders of these hairpins can, on occasion, pinch off at their legs, eventually leading to detachment of their omega portions. When such a process occurs, the detached omega portions are then observed to reconnect and form ring-like structures. Simultaneously, spanwise-oriented vortical 'bridges' appear to form between the remaining legs (figure 11 in Bake *et al.* 2002). If one were to slice through this pattern with a streamwise–wall-normal measurement plane, one would observe a signature similar to that highlighted in figure 7 (an instantaneous velocity realization from the present PIV ensemble): a retrograde spanwise vortex (B) bounded by prograde cores both below (A) and above (C). In such a scenario, the prograde core above the retrograde structure would be associated with the detached ring-like structure while the prograde core below

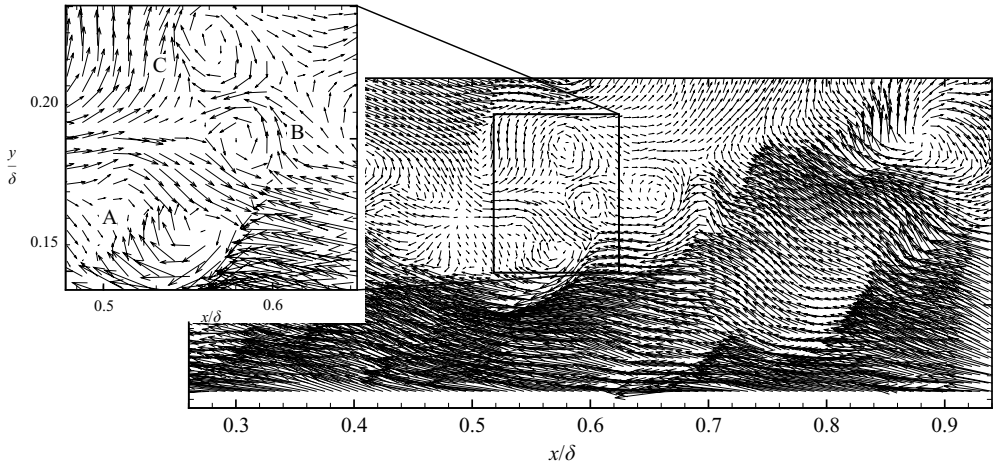


FIGURE 7. Example of a prograde hairpin vortex head (labelled A) oriented at approximately 255° relative to a neighbouring retrograde vortex (labelled B), as visualized by Galilean decomposition of an instantaneous velocity realization with $U_c = 0.79U_\infty$.

would represent the imprint of the spanwise vortical 'bridge' that forms between the remaining legs of the original hairpin. Further analysis, preferably with time-resolved three-dimensional data at moderate *Re*, would shed additional light on the preferred orientations observed herein.

This work was performed with funding from the Air Force Office of Scientific Research under Grants FA9550-05-1-0043 and FA9550-05-1-0246 (Dr. John Schmisseur, Program Manager) and the University of Illinois.

## REFERENCES

ADRIAN, R. J., MEINHART, C. D. & TOMKINS, C. D. 2000 Vortex organization in the outer region of the turbulent boundary layer. *J. Fluid Mech.* **422**, 1–54.

BAKE, S., MEYER, G. W. & RIST, U. 2002 Turbulence mechanism in Klebanoff transition: A quantitative comparison of experiment and direct numerical simulation. *J. Fluid Mech.* **459**, 217–243.

CHRISTENSEN, K. T., WU, Y., ADRIAN, R. J. & LAI, W. 2004 Statistical imprints of structure in wall turbulence. *AIAA Paper* 2004-1116.

FALCO, R. E. 1977 Coherent motions in the outer region of turbulent boundary layers. *Phys. Fluids* **20** (10), S124–S132.

FALCO, R. E. 1983 New results, a review and synthesis of the mechanism of turbulence production in boundary layers and its modification. *AIAA Paper* 83-0377.

FALCO, R. E. 1991 A coherent structure model of the turbulent boundary layer and its ability to predict Reynolds number dependence. *Phil. Trans. R. Soc. Lond.* A **336**, 103–129.

GANAPATHISUBRAMANI, B., LONGMIRE, E. K. & MARUSIC, I. 2003 Characteristics of vortex packets in turbulent boundary layers. *J. Fluid Mech.* **478**, 35–46.

HAMBLETON, W. T., HUTCHINS, N. & MARUSIC, I. 2006 Simultaneous orthogonal-plane particle image velocimetry measurements in a turbulent boundary layer. *J. Fluid Mech.* **560**, 53–64.

HEAD, M. R. & BANDYOPADHYAY, P. 1981 New aspects of turbulent boundary-layer structure. *J. Fluid Mech.* **107**, 297–338.

KLEWICKI, J. C. & HIRSCHI, C. R. 2004 Flow field properties local to near-wall shear layers in a low Reynolds number turbulent boundary layer. *Phys. Fluids* **16**, 4163–4176.

Meinhart, C. D. 1994 Investigation of turbulent boundary-layer structure using particle-image velocimetry. PhD thesis, Department of Theoretical and Applied Mechanics, University of Illinois at Urbana-Champaign.

Moin, P., Leonard, A. & Kim, J. 1986 Evolution of a curved vortex filament into a vortex ring. *Phys. Fluids* **29**, 955–963.

Nagaosa, R. & Handler, R. A. 2003 Statistical analysis of coherent vortices near a free surface in a fully developed turbulence. *Phys. Fluids* **15**, 375–394.

Smith, C. R., Walker, J. D. A., Haidari, A. H. & Sobrun, U. 1991 On the dynamics of near-wall turbulence. *Phil. Trans. R. Soc. Lond* A **336**, 131–175.

Theodorsen, T. 1952 Mechanism of turbulence. In *Proc. 2nd Midwestern Conference on Fluid Mechanics*, pp. 1–19. Ohio State University, Columbus, Ohio.

Tomkins, C. D. & Adrian, R. J. 2003 Spanwise structure and scale growth in turbulent boundary layers. *J. Fluid Mech.* **490**, 37–74.

Wu, Y. & Christensen, K. T. 2006 Population trends of spanwise vortices in wall turbulence. *J. Fluid Mech.* **568**, 55–76.

Zhou, J., Adrian, R. J., Balachandar, S. & Kendall, T. M. 1999 Mechanisms for generating coherent packets of hairpin vortices in channel flow. *J. Fluid Mech.* **387**, 353–396.